IEEE Access
Multidisciplinary ⋮ Rapid Review ⋮ Open Access Journal

Date of publication xxxx 00, 0000, date of current version xxxx 00, 0000.

Digital Object Identifier 10.1109/ACCESS.2017.Doi Number

A Wide-Angle, Polarization-Insensitive, Wideband Metamaterial Absorber with Lumped Resistor Loading for ISM Band Applications

ABDULRAHMAN AHMED GHALEB AMER [1], SYARFA ZAHIRAH SAPUAN [1], NURMIZA OTHMAN[1], ALI AHMED SALEM[2], AHMED JAMAL ABDULLAH AL-GBURI[3] AND ZAHRILADHA ZAKARIA[3]

[1] Faculty of Electrical and Electronic Engineering, Universiti Tun Hussein Onn Malaysia, UTHM, Batu Pahat 86400, Johor, Malaysia
[2] School of Electrical Engineering, College of Engineering, Universiti Teknologi MARA (UITM), 40450, Shah Alam, Selangor, Malaysia.
[3] Center for Telecommunication Research & Innovation (CeTRI), Fakulti Teknologi dan Kejuruteraan Elektronik dan Komputer (FTKEK), Universiti Teknikal Malaysia Melaka (UTeM), Jalan Hang Tuah Jaya, Durian Tunggal, Melaka 76100, Malaysia

Corresponding authors: Zahriladha Zakaria (zahriladha@utem.edu.my) and Ahmed Jamal Abdullah Al-Gburi (ahmedjamal@ieee.org)

ABSTRACT This work introduces a wideband metamaterial (MM) absorber designed to operate effectively across a wide reception angle and be polarization-insensitive within ISM band (2.4 GHz) applications. The proposed absorber unit cell comprises four copper sectors loaded with lumped resistors and a full copper ground plane hosted onto two FR4 substrates. Furthermore, an air layer suspended between the ground plane and a FR4 substrate is applied to achieve wideband absorption. In addition, the simulation results show that particular design factors, such as lumped resistors and unit cell geometry, can be optimized to improve the efficiency of the absorber. The simulations demonstrate that the proposed absorber achieves a wideband absorption, exceeding 90%, over a broad frequency range from 1.94 GHz to 2.98 GHz. The designed absorber was fabricated and tested, and the simulation and measurement results were agreed well.

INDEX TERMS Electromagnetic absorber, metamaterial (MM), polarization independent, wideband.

I. INTRODUCTION

Electromagnetic (EM) wave absorbers, known as blackbodies, have garnered significant attention due to their ability to prevent the reflection and transmission coefficients of EM radiation, making them highly used in real-world applications, including Electromagnetic compatibility (EMC) and stealth techniques, etc. Recently, MM comprised of artificially engineered subwavelength structures has been shown to have great ability in designing microwave absorbers due to their unique properties, such as negative permittivity, negative permeability, and refractive index [1]. Due to these extraordinary properties, MMs are used in various applications, including invisibility cloaking [2], imaging [3], super lens [4], sensors [5],[6], absorbers [7]–[11], energy harvesting [12]–[14]. Therefore, MM absorbers attracted much attention from researchers worldwide due to their various applications for several on-demand needs. In particular, microwave absorbers can be used to reduce the radar cross-section (RCS) and EM interference (EMI) [15], [16]. Unlike conventional absorbing materials such as ferrite [17], near-unity absorption can be achieved by fabricating MMs in a thin configuration and using low-cost printed circuit boards (PCBs). The progress in MM absorber design has successfully overcome the drawbacks associated with conventional material absorbers, which often suffer from issues like bulkiness, large size, and higher thickness. Landy et al.2008 [18] produced the concept of the perfect MM absorber with a compact and ultrathin structure, achieving a near-unity absorption by effectively effective impedance matching between the absorber and free space. MM absorbers have been developed in a variety of frequency ranges, including single band[19], [20], dual band[21], [22], and multiband [23]–[25].

However, the operational concept of MM absorbers depends on resonator arrays; therefore, their absorption is frequency-dependent, and they have a narrow absorption bandwidth [26]. For most applications, the absorbers with a wide bandwidth absorption are preferred. Thus, various techniques are used to increase the bandwidth of the MM absorbers, including the use of multilayers [27]–[30], multi-resonant [31], [32] techniques. However, these methods have produced some drawbacks, such as increased total thickness,

assembly difficulties, and a possibility for discrete absorption bands. Another method to design a broadband metamaterial absorber is using silicon and graphene-based materials. However, the cost can be quite high, and the fabrication process is complex [33], [34]. An alternative method to achieve a wide absorption bandwidth is to use the MM absorbers with lumped resistors mounted between the splits of the top metallic layer. This is due to the resistors providing extra ohmic losses in the metallic surface [35]–[37]. However, the losses introduced by the lumped resistors might not suffice to achieve a sufficiently wide absorption bandwidth. Fortunately, this challenge can be addressed by designing the absorber with a layer of flexible foam (air gap) or rubber placed between the substrate and ground plane [38]–[47]. In [38], an MM absorber loaded with four lumped resistors and an air layer is designed over a frequency range from 860 to 960 GHz, achieving a relative bandwidth of 14%. In addition, an MM absorber with angular stability is designed to operate over a wideband frequency range from 3 GHz to 10 GHz. To achieve an effective broadband absorption, eight resistor loads and an air layer are applied in the absorber design [43]. In [46], a wideband MM absorber is designed to operate within a frequency range of 1.44 GHz to 6.32 GHz. In the absorber design, eight resistors, and an air layer are applied to realize broadband absorption.

The main contributions in this paper can be concisely summarized as follows:

1. Design and analysis of a wideband metamaterial absorber for ISM application (2.4 GHz).
2. A near-unity absorption of about 99.99% is achieved at the operating frequency of 2.4 GHz.
3. A wider 90% absorption bandwidth over 1 GHz is achieved within the frequency band of 1.94 GHz to 2.99 GHz.

This paper introduces a conformal MM absorber with integrated resistors, offering angular stability and polarization insensitivity over a wideband frequency range. The proposed MM absorber comprises a lumped resistor loaded-cross-shaped resonator on the top side and a copper plate separated by an air layer on the back side of the substrate. Numerical results demonstrate that the proposed absorber achieves a higher absorptivity of about 90% within the frequency range of 1.94 GHz to 2.98 GHz. Moreover, it exhibits an increased absorption ratio at various incident angles for both TE and TM polarizations. CST Microwave Studio is used to analyze the surface current density electric and magnetic field distributions within the unit cell to gain a deeper insight into the absorption mechanism. Finally, the designed MM absorber was fabricated and examined to confirm its capability to meet the absorption requirements within the designed frequency band.

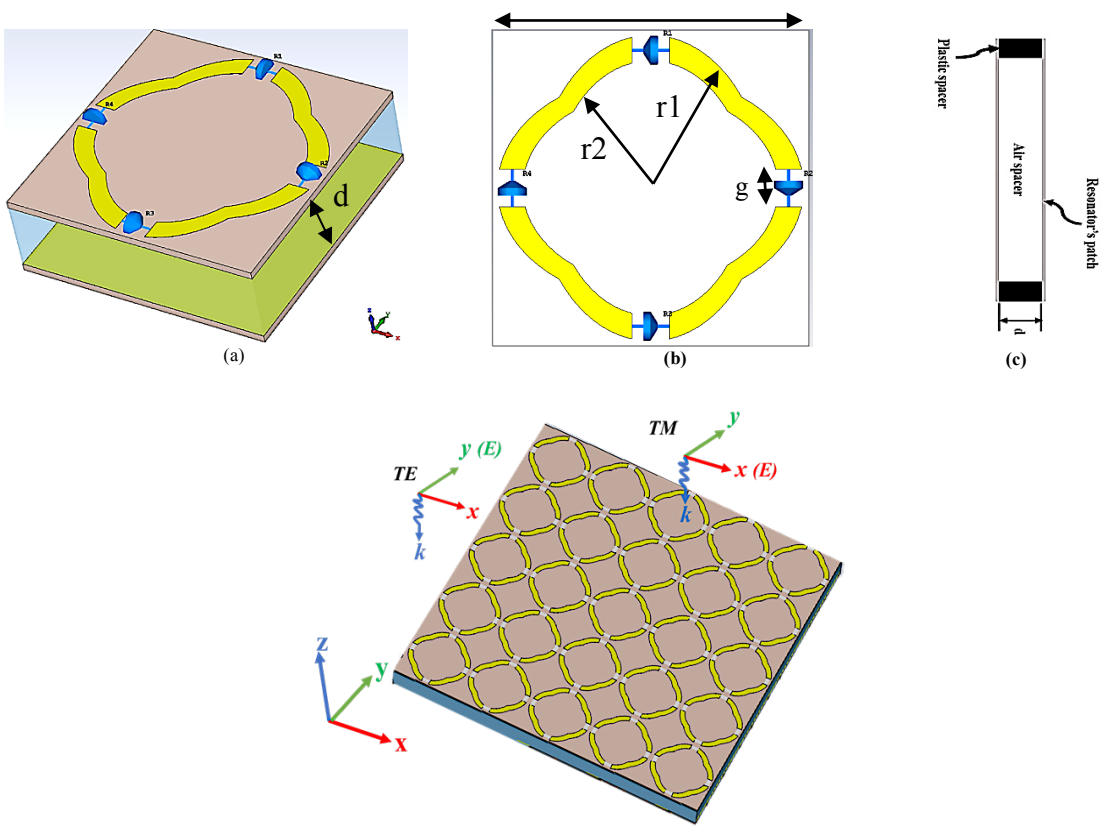

FIGURE 1. MM absorber (a): 3D view, (b) top view, (c) side view, and (d) schematic diagram of the absorber.

II. METAMATERIAL ABSORBER DESIGN

A unit cell of the proposed MM energy absorber is shown in Fig. 1. The proposed MM unit cell comprises interconnected double metallic elliptical resonators that incorporate lumped resistor loads. The dielectric substrate comprises of FR4 with a thickness of 1.6 mm, a dielectric constant of 4.3, and a tangent loss of 0.025. The 2-D structure of the unit cell is depicted in Fig. 1(b), and the dimension parameters were optimized as follows: $P = 55.7$ mm, $r1 = 27$ mm, $r2 = 20$ mm. The incident EM power is captured and concentrated within the resonator's splits (g), where $g = 6.5$ mm. Four lumped resistor loads are placed across the resonator's splits to examine the MM unit cell's capability of capturing and consuming collected EM power. The optimized resistance of the lumped resistors is 550 Ω. A ground plane is positioned with an ideal standoff distance of d = 15 mm from the substrate's bottom side, as shown in Fig. 1(c). The metallic material used herein is copper with conductivity of 5.8×10^7 S/m and thickness of 35μm. Fig. 1(d) shows specific details regarding the incident wave. CST Microwave Studio is used with periodic boundary (unit cell boundary) conditions to simulate the cell as a large structure with transverse electromagnetic (TEM) excitation. The unit cell boundary conditions for TE and TM modes are implemented to the x- and y-axes, while open boundaries are applied to the z-axis. Floquet ports with TE and TM modes are used for excitation along with the z-axis.

III. RESULTS AND DISCUSSION

First, in the simulation configuration, the air space distance (d) between the resonator patch and ground plane was adjusted from 5 mm to 20 mm with 5 mm increments. Subsequently, the lumped resistors were swept from R= 400 Ω to R= 600 Ω across all four-spacer distances. The reflection coefficient of the proposed MM absorber was then calculated. The simulated reflection coefficient of the MM absorber is presented in Fig. 2(a)-(d), corresponding to different lumped resistors spanning from R = 400 Ω to R = 600 Ω, and with spacer distances of d = 5 mm, d = 10 mm, d = 15 mm, and d = 20 mm, respectively. It is observed that as the separation distance (d) increases, the resonance frequency shifts to lower frequencies. This phenomenon can be explained using equation (1), which indicates that the resonance frequency changes as the capacitance and inductance values change.

$$f = \frac{1}{\sqrt{LC}} \tag{1}$$

Based on this investigation, the lowest reflection of < 40 dB at 2.4 GHz is achieved when the proposed MM structure is terminated by resistor loads of $R = 550$ Ω at the separation distance of $d = 15$ mm, as shown in Fig. 2(c).

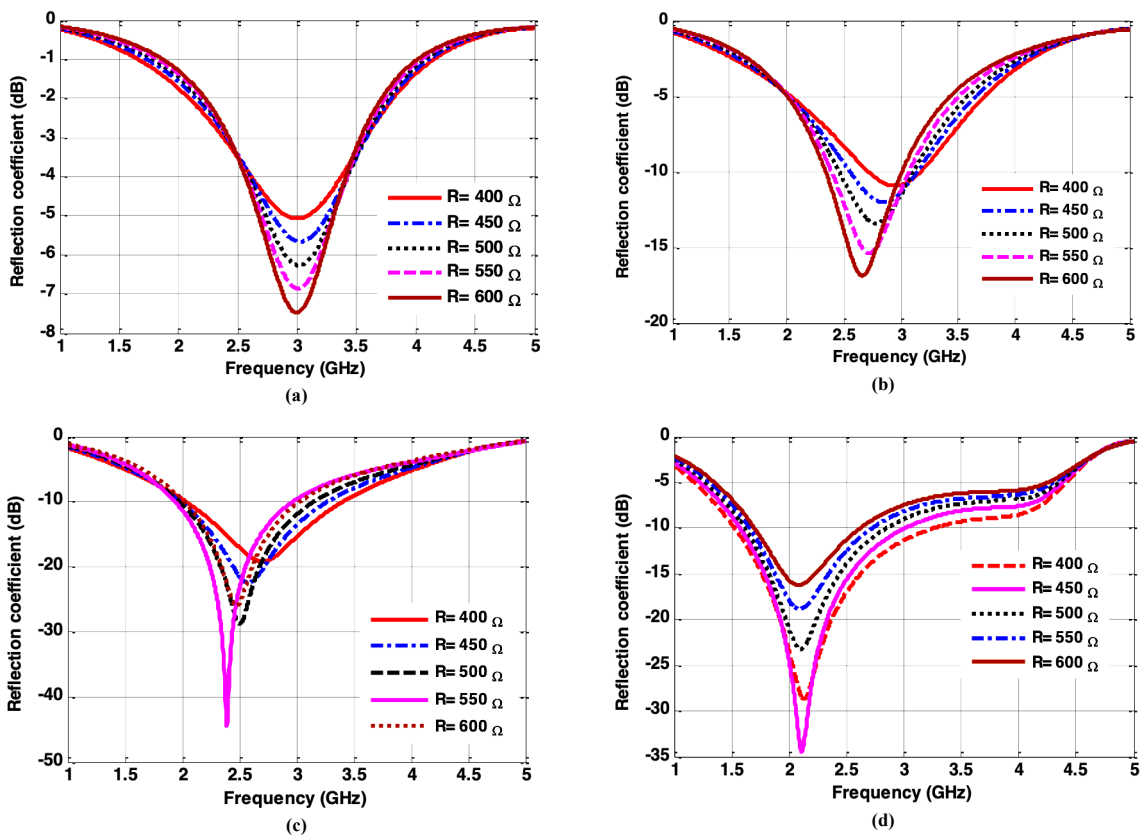

FIGURE 2. Simulation results illustrate the reflection coefficient of the proposed MM absorber under different resistor loads spanning from 400 Ω to 600 Ω, and with air spacer distances of (a) d= 5 mm, (b) d= 10 mm, (c) d= 15 mm and (d) d= 20 mm.

Mathematically, the absorptivity can be described by equation (2).

$$A(\omega) = 1 - R(\omega) - T(\omega) \quad (2)$$

where $T(\omega)$ are the reflected power and transmitted power, respectively. To optimize absorptivity, it is essential for both reflected and transmitted power to be minimized. The transmitted power $T(\omega) = 0$ is almost zero due to the full ground plane. Fig. 3 depicts the proposed MM absorber's simulated absorption, reflection, and transmission curves. Fig. 3 shows the proposed MM absorber's simulated absorption, reflection, and transmission curves. It is evident that a near-unity absorption of about 99.99% is achieved at 2.4 GHz. Furthermore, a 90% wideband absorptivity is obtained over the frequency band of 1.94 GHz to 2.99 GHz.

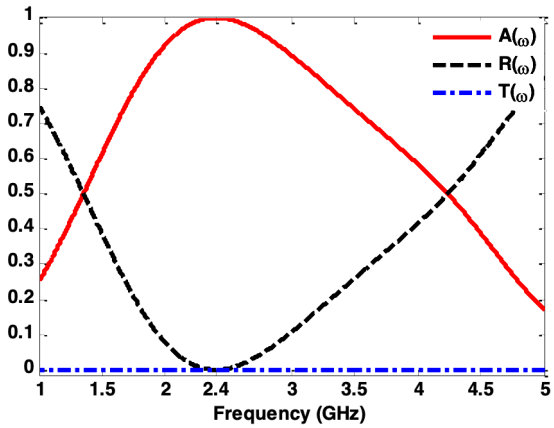

FIGURE 3. Simulated absorption, reflection, and transmission coefficients.

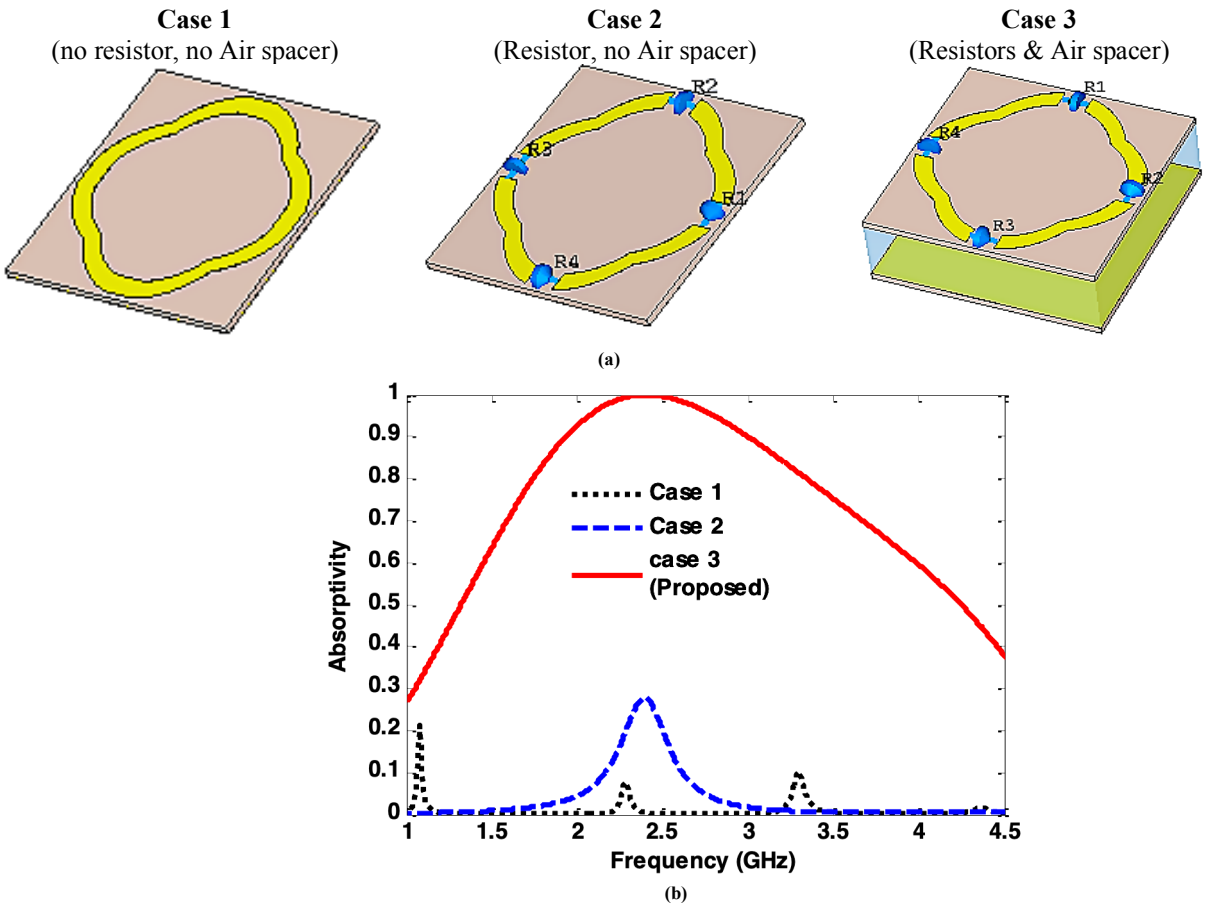

FIGURE 4. (a) Diagram of the stages of the absorber's design and (b) Simulated absorption responses of each stage

A. EVALUATION OF THE DESIGN CONCEPT

To study the impact of lumped resistors and air spacer on absorptivity, three cases of proposed MM absorbers have been numerically investigated, as shown in Fig. 4.

Case 1: the initial design proposed by double elliptical resonators hosted on the top side surface of a thicker FR4 substrate with a metal backing. A low absorptivity of about 20%, less than 10%, is observed at 1.07 GHz, 2.3 GHz, and 3.3 GHZ, respectively. In this configuration, only dielectric losses enable the resonance of three narrow frequency bands without significant absorption. Nevertheless, the purpose of this structure is to adjust the original operating frequency and subsequently enhance the bandwidth in the following steps.

Case 2: Four lumped resistors are inserted between the splits of the resonator (R= 590 Ω), as shown in Fig. 4a (case 2). At the resonance frequency of 2.4 GHz, the absorption of the EM wave increased due to additional energy loss caused by ohmic losses in the resistors.

Finally, to achieve a higher absorptivity with a wider bandwidth, an air space between the ground plane and the dielectric substrate is placed, as shown in Fig. 4(a) (case 3). It is realized that a near unity absorption with wider bandwidth is observed, as depicted in Fig. 4(b). The result can be stated as follows: adding the air spacer caused a decrease in effective permittivity, consequently increasing the bandwidth of absorption. The resistance value was adjusted to achieve a higher absorption value with a wider bandwidth. Fig. 4(c) demonstrates that, in contrast to cases 1 and 2, this absorber achieves a near-unity absorption level of about 99.99% at 2.4 GHz. Furthermore, a 90% wider absorption bandwidth is achieved within the frequency band of 1.94 GHz to 2.99 GHz.

The equivalent circuit of the proposed absorber is shown in Fig. 5. It comprises three sections. Section A is the patch (metallic elliptical resonator), which consists of the parallel capacitor (C), inductor (L), and resistor (R). Section B represents the top substrate layer (FR4), and Section C represents the air spacer with thickness d. The coupling between the top metallic elliptical resonator and the ground plane is not considered because a large spacer d separates them. According to the transmission line model, the input impedance of the proposed MM structure can be calculated as

$$Z_m = (C_e + L_e + R_e) \,||\, Z_2 \tag{3}$$

$$Z_2 = Z_h \frac{Z_1 + Z_h \tanh \gamma d}{Z_h + Z_1 \tanh \gamma d} \tag{4}$$

$$Z_1 = jZ_o \tan \beta d \tag{5}$$

where Z_h and Z_o is the impedance of the FR4 substrate and air layer, respectively. γ and β are the propagation constant and phase constant of the air layer. The effective capacitor (C_e), inductor (L_e), and resistor (R_e), extracted from the Keysight Advanced Designs System (ADS) simulator, are determined in Table I.

TABLE I
ADS VALUE OF R, L, C

Parameter	*Value*
C_{e1}	*0.65 pF*
C_{e2}	*0.2 pF*
L_{e1}	*22.7 nH*
L_{e2}	*4.45 nH*
R_{e1}	*105 Ω*
R_{e1}	*77 Ω*

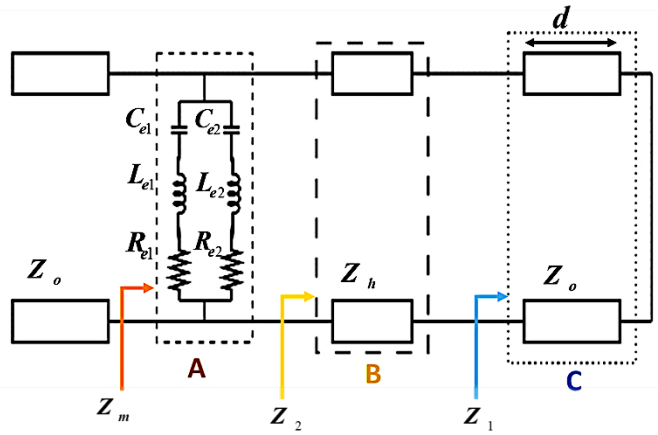

FIGURE 5. Equivalent Circuit

The results obtained from ADS were compared with those simulated in CST, demonstrating a reasonable agreement that validates the structure's equivalent circuit model, as depicted in Fig. 6.

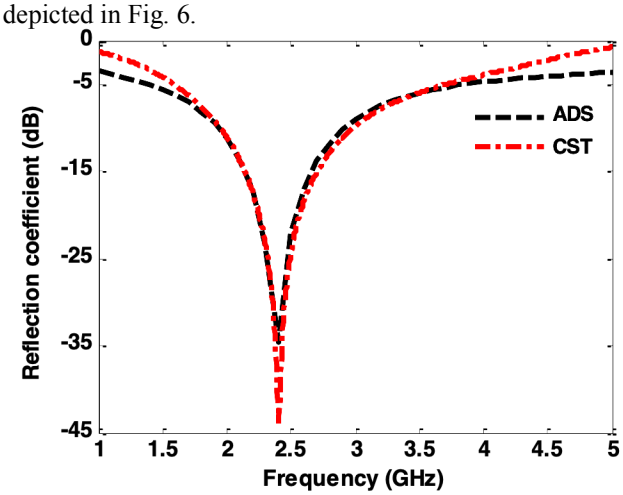

FIGURE 6. Comparison of the simulated absorptivity of CST and ADS results.

The absorptivity of the proposed MM absorber under various conditions is investigated and plotted in Fig. 7. Fig. 7(a) illustrates the absorption of the absorber with TE and TM polarization under normal incidence. The proposed absorber achieved a near unity absorption with a wider bandwidth regardless of the polarization mode. Fig. 7(b) shows the absorption curves under free loss and low loss conditions of the substrate material (FR4), where a near unity absorption is observed. Furthermore, Fig. 7(c) illustrates the absorption curves of the MM absorber both with loaded and unloaded lumped resistors. The MM absorber with unloading lumped resistors showed fourth absorption peaks of 70%, 97%, 58%, and 97% at 1.15 GHz, 3.35 GHz, 3.77 GHz, and 4.43 GHz, respectively. The simulated results show that the lumped resistor is critical in achieving a near unity absorption and wider bandwidth.

This article has been accepted for publication in IEEE Access. This is the author's version which has not been fully edited and content may change prior to final publication. Citation information: DOI 10.1109/ACCESS.2023.3345659

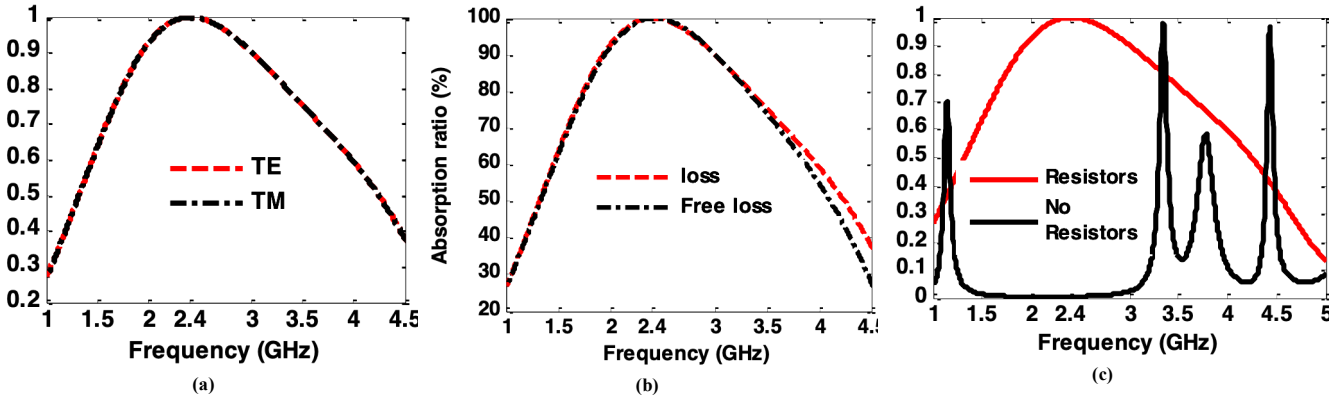

FIGURE 7. Absorption spectrum under various conditions: (a) Absorption for TE and TM polarization, (b) Absorptivity in two different loss situations, and (c) Absorptivity for loading and unloading resistor loads.

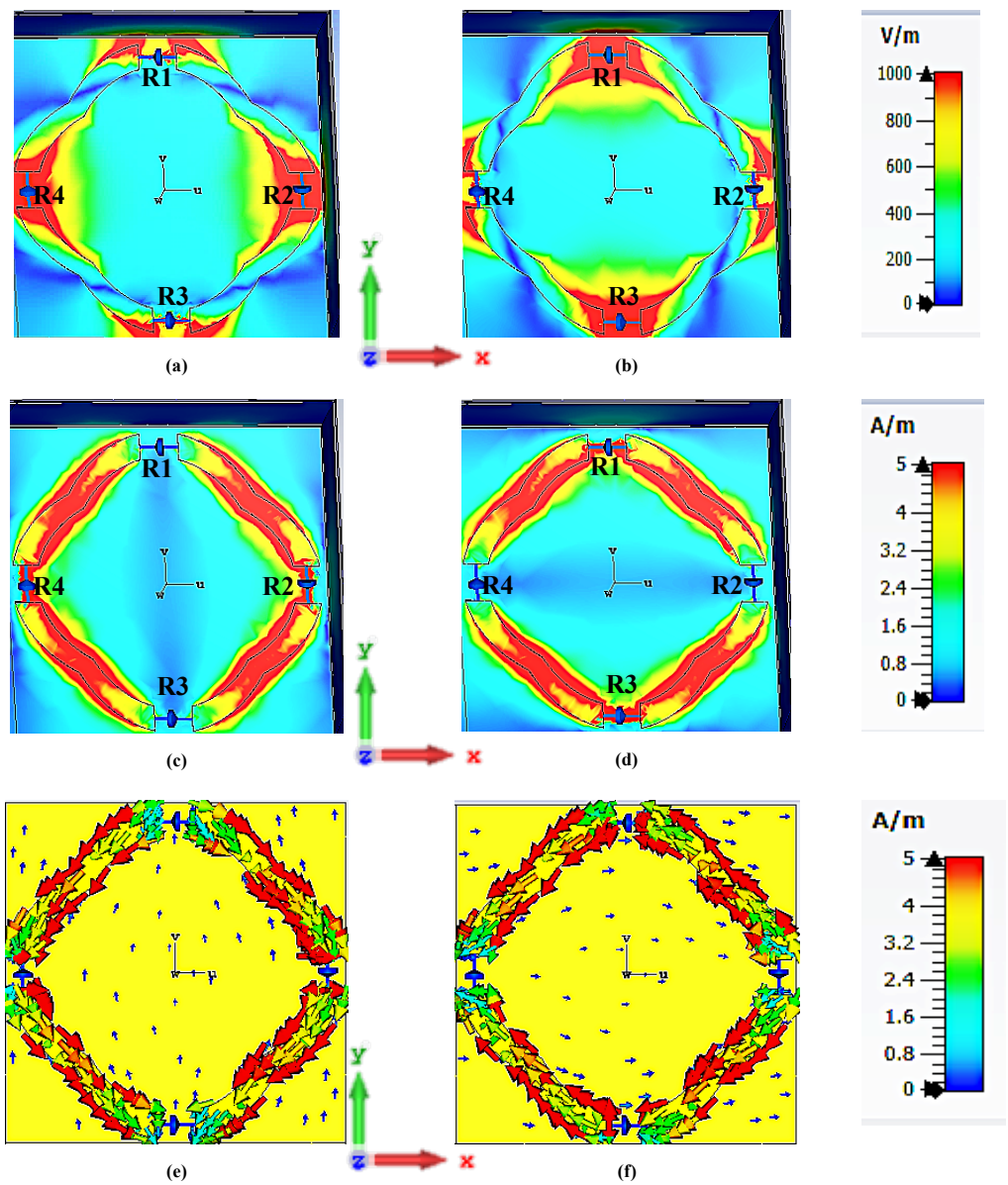

FIGURE 8. (a, b) E-field for TE and TM modes, (c, d) H-field for TE and TM modes, and (E, F) surface current for TE and TM modes, respectively, for the proposed MM absorber at 2.4 GHz.

The design principle of the proposed MM resonator relies on the generation of electric and magnetic fields induced by the interaction with EM waves. Magnetic fields (H-field) are produced when opposite currents are introduced into the upper and lower metal layers. The electric field (E-field) can be enhanced by focusing on the absorber's upper surface. The maximum absorption is achieved when electric and magnetic excitation occur simultaneously. The surface current, E-field, and H-field distributions for the MM absorber at 2.4 GHz for TE and TM polarizations are investigated to emphasize the absorption performance, as shown in Fig. 8. Fig. 8(a) and (b) show the E-field of the proposed MM absorber for TE and TM polarizations, respectively. The E-field is intense at the edges of the four resistor's splits and more concentrated at the resistor loads of (R2 and R4) across the x-axis for TE polarization and (R1 and R4) across the y-axis for TM polarization, a contributor to the permittivity. The H-field distribution is shown in Fig. 8(c) and (d). It is distributed along the resonator contributing to the permeability, and concentrated across the (R2 and R4) across the x-axis for TE polarization and (R1 and R4) across the y-axis for TM polarization. The surface current distribution is antiparallel for both TE and TM modes and concentrated around the resistor loads, as shown in Fig. 8(e) and (f).

B. Absorptivity at Various Incident and Polarization Angles

In practical situations, the orientation of the incident EM wave remains uncertain. Therefore, an MM absorber's Angular stability is an essential aspect of its efficiency. Therefore, good absorption efficiency at different polarization and incident angles is desirable. To evaluate the polarization efficiency of the MM absorber, the E-field and H-field directions are rotated at various polarization angles (ϕ) in the step of 30^o, while maintaining the direction of the EM wave. Fig. 9 depicts the absorption curves of the MM absorber at different polarization angles ranging from 0^o to 90^o. According to Fig. 9, due to the symmetrical design of the MM absorber, absorptivity remains consistent across a range of polarization angles for both TE and TM polarizations.

As shown in Fig. 9, the absorptivity response for the absorber remains almost the same at different polarization angles (ϕ), indicating that it is polarization insensitive. To further investigate whether the proposed MM structure functions as an absorber or converter, the polarization conversion ratio (PCR) is examined. The PCR can be calculated using equation (6) [48]

$$PCR = \frac{|r_{yx}|^2}{|r_{yx}|^2 + |r_{xx}|^2} = \frac{|r_{xy}|^2}{|r_{xy}|^2 + |r_{yy}|^2} \qquad (6)$$

where, $r_{yx} = E_{yx}/E_{xi}$ and $r_{xx} = E_{xr}/E_{xi}$ are the cross and co-polarized reflection coefficients for x-polarization incidence, whereas the cross and co-polarized reflection coefficients for y-polarization angle are $r_{xy} = E_{xr}/E_{yi}$, and $r_{yy} = E_{yr}/E_{yi}$, respectively, where the indices 'i' and 'r' represent incident and reflected waves, respectively. Fig. 10 shows the simulated co- and cross-polarized reflection and PCR for the MM structure. It is observed that the PCR is nearly zero, affirming that the structure functions as an absorber rather than a converter.

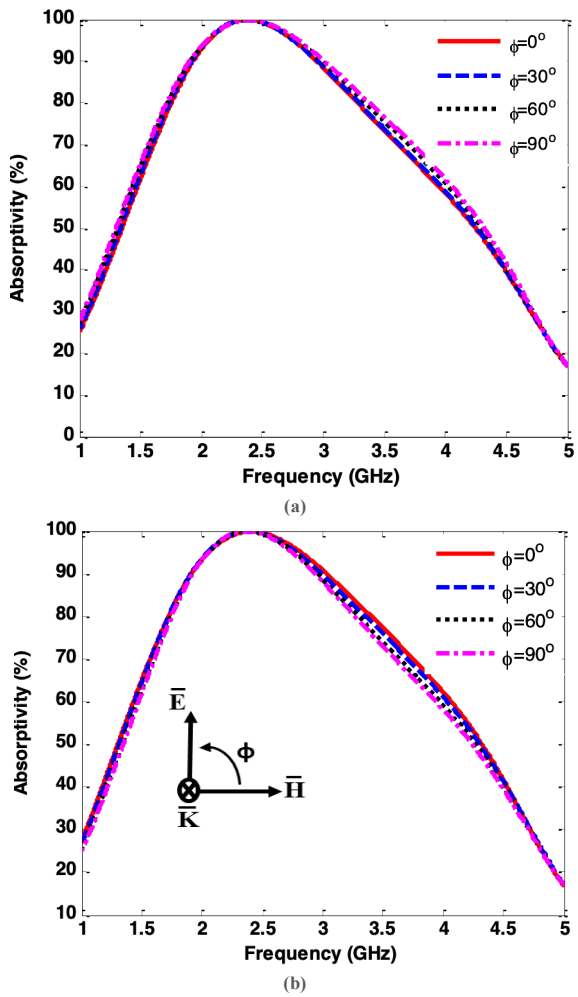

FIGURE 9. Absorptivity at different polarization angles (a) TE and (b) TM mode

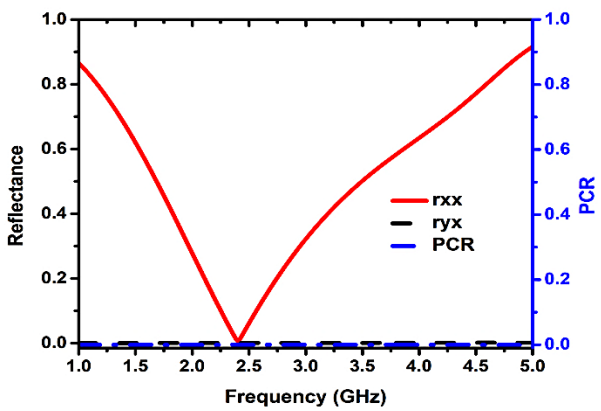

FIGURE 10. Co- and cross-polarized reflection and PCR under x polarized angle.

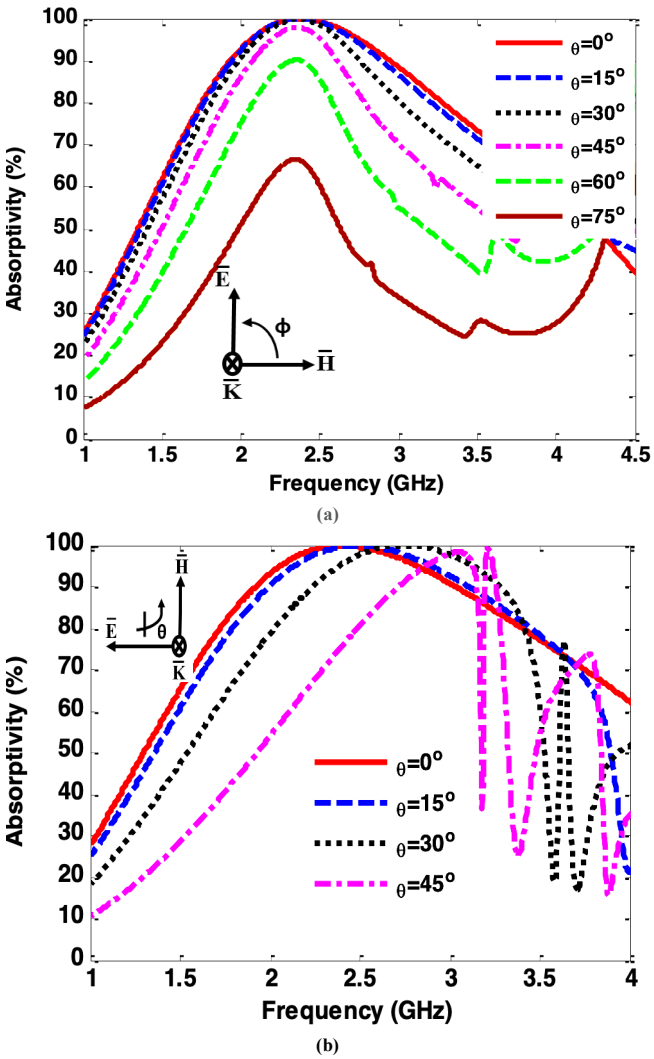

FIGURE 11. Absorption for various incident angles (a) TE polarization and (b) TM polarization

At oblique incidence, the reflection coefficient (Γ) for TE and TM polarization can be described as follows.

$$\Gamma_{TE} = \frac{z(\omega)\cos\theta_i - z(\omega)\cos\theta_t}{z(\omega)\cos\theta_i + z(\omega)\cos\theta_t} \quad (7)$$

$$\Gamma_{TM} = \frac{z(\omega)\cos\theta_t - z(\omega)\cos\theta_i}{z(\omega)\cos\theta_t + z(\omega)\cos\theta_i} \quad (8)$$

where θ_i and θ_t are the incident and transmitted angles, respectively. The absorptivity of the proposed MM absorber is examined at different incident angles for both TE and TM polarizations and presented in Fig. 9. Both TE and TM polarization are considered. Based on equations (7) and (8), the reflection changes as the incident angle varies. Fig. 11 illustrates the absorptivity of the MM absorber for various incident angles for TE and TM polarizations. In TE polarization, the electric field remains constant in direction, but the focus of EM and magnetic field rotates as the incident angle changes, as depicted in Fig. 11(a). The absorptivity decreases as the incident angle increases, but the absorptivity exceeds 65% up to the incident angle 75^o. In TM polarization, the direction of the H-field remains constant. In contrast, the E-field's focus and the EM wave's propagation direction rotate at different incident angles, as shown in Fig. 11(b). It is noted that the resonance frequency shifts as the incident angle increases and the bandwidth decreases. Furthermore, parasitic resonances generate extra absorption peaks that rise significantly as the incident angle increases. However, the absorptivity is still over 75 % at 2.4 GHz up to the incident angle of 45^o.

C. Parametric study

Several critical parameters that influence the efficiency of the MM absorber were investigated and analyzed to assess the stability of the proposed MM absorber. Fig. 12 shows the absorptivity at different design parameters, including air layer height (*d*), inner radius (*r2*), the resistance value of the lumped resistor (*R*), and the split gap length (*g*)**.** Fig. 12(a) shows the absorption ratio as the air layer height (h) varies from 0 to 15 mm in the step of 5 mm. As the parameter h increases, the resonant frequency shifts to the left while the reflection coefficient remains below 10 dB. The parameter h is chosen at 15 mm as the MM structure has achieved a reflection efficiency of less than 10 dB across the frequency range 1.94 GHz to 2.99 GHz. The reflection curves in Fig. 12(b) illustrate changes as the inner resonator's radius (r2) varies from 16 mm to 22 mm in 2 mm increments—obviously, the relative bandwidth increases as the parameter r2 increases. The minimum reflection and wider relative bandwidth are observed when the parameter r2 equals 20 mm. Fig. 12(c) shows the reflection coefficient when the lumped resistor value changes from 400 Ω to 600 Ω. The minimum reflection is achieved when the resistor load value equals 560 Ω, leading to a near unity absorption of more than 99.99% at 2.4 GHz. In addition, the impact of the split length parameter (g) on the reflection is investigated and plotted in Fig. 12(d). It is clear that as the split length (g) increases, the resonance frequency shifts to the right side due to the change values of the capacitor and inductor, as explained in Eq. (1). The split length is chosen at g= 6.65 mm.

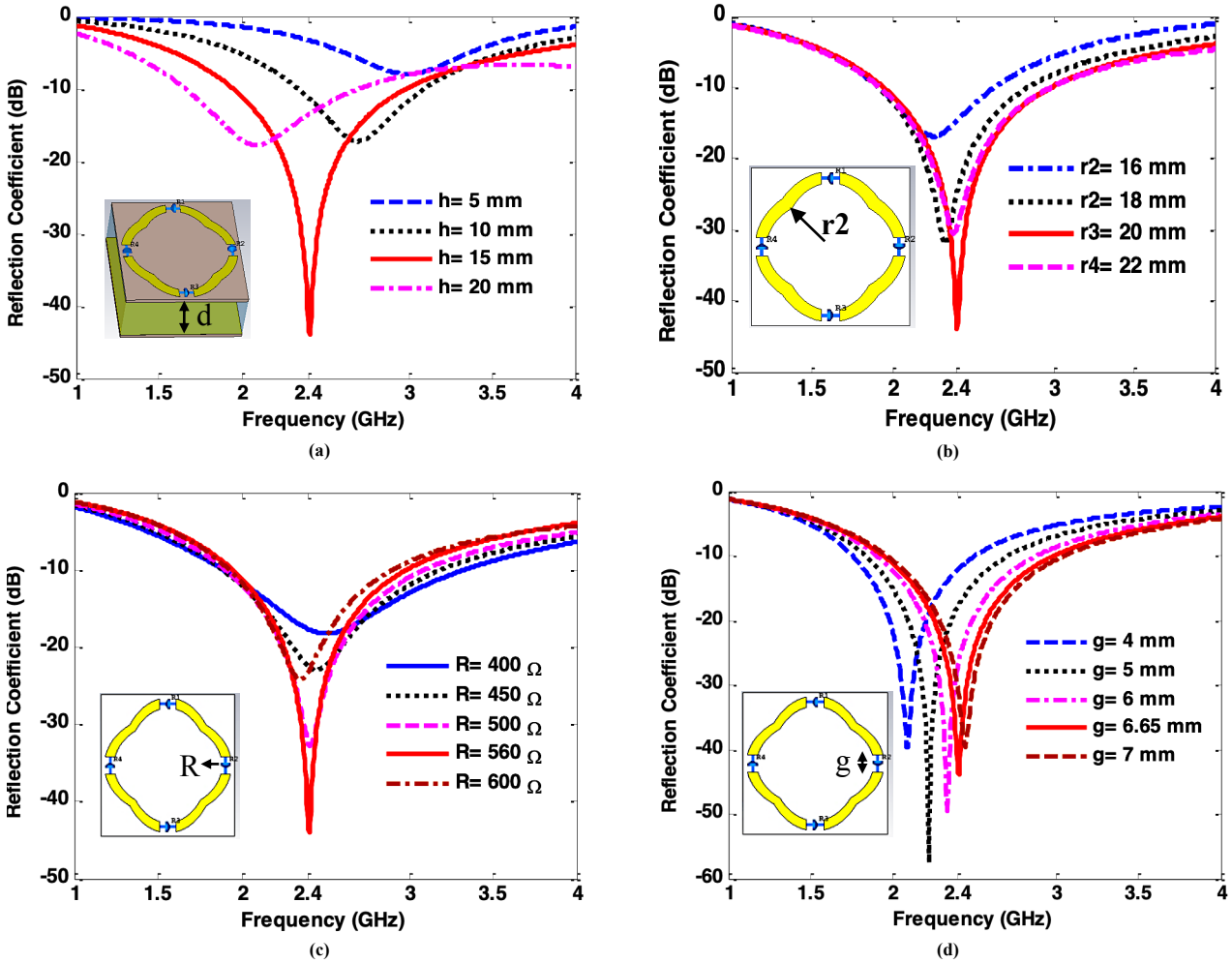

FIGURE 12. The absorption spectrum of the MM absorber with different geometrical parameters (a) air layer height (h), (b) inner resonator radius (r2), (c) lumped resistor (R), and (d) splits of the resonators (g).

D. Measurement Procedures

As a further step, the proposed MM absorber is experimentally verified by measuring the absorption of the large array. First, the proposed MM absorber is fabricated using conventional printed circuit board technology (PCB) using the same MM unit cell dimensions as in the simulation. Then, the lumped resistors were loaded onto the electric resonator structure using welding technology.

As proof of concept, an array MM absorber with dimensions of 278.5 mm ×278.5 mm, containing 25 identical unit cell structures, was produced as shown in Fig. 13(a).

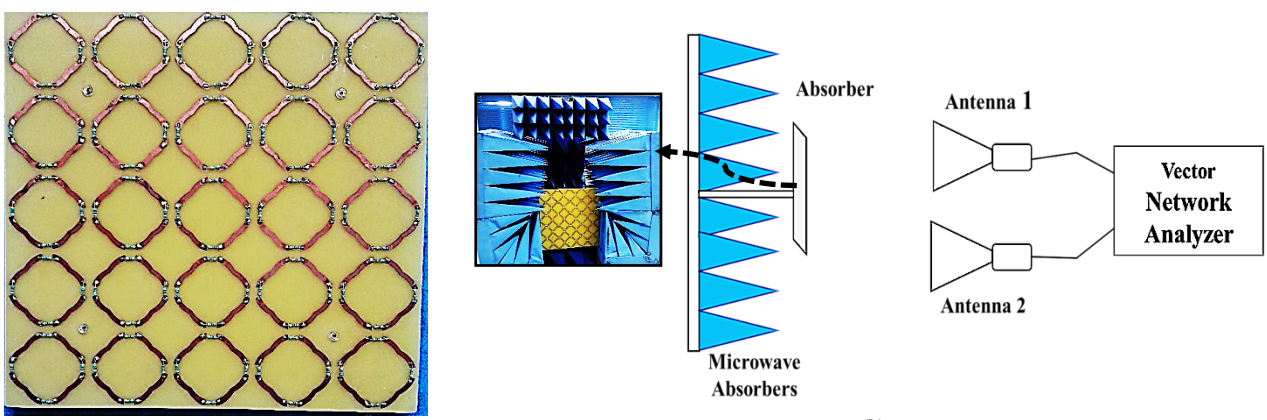

FIGURE 13. (a) Fabricated MM absorber and (b) measurement experimental setup

Fig. 13(b) depicts the measurement setup. The measurement of the reflection coefficient for the fabricated MM array was conducted using a vector network analyzer (VNA) connected to two horn antennas (HF906 type) serving as the transmitter and receiver. The fabricated MM array is placed $>2D^2/\lambda$ away from the horn antennas to fulfill the far-field condition. Initially, the reflection from the metal plate is measured, followed by the placement and measurement of the fabricated sample. The difference between these measurements represents the true reflection of the fabricated MM absorber.

Fig. 14 shows the MM absorber's simulated and measured absorption characteristics under normal incidence. It is evident that the measured absorptivity closely matches the simulation results, confirming the accuracy and reliability of the theoretical model. The minor difference observed can be attributed primarily to fabrication tolerances, precisely the air layer's height and the measurement setup's environment. The measured absorptivity exceeding 90% is achieved across the frequency band of 1.87 GHz to 2.51 GHz. This significant absorption performance indicates that the absorber has Potential for use in applications requiring high-efficiency EM wave absorption in this frequency range. The achievement of such significant absorption levels emphasizes this MM absorber's potential applications in various technological fields, including electromagnetic interference mitigation, radar technologies, and communication systems. However, it is essential to recognize the presence of additional absorption attributed to parasitic resonances arising from the measurement environment and fabrication tolerances.

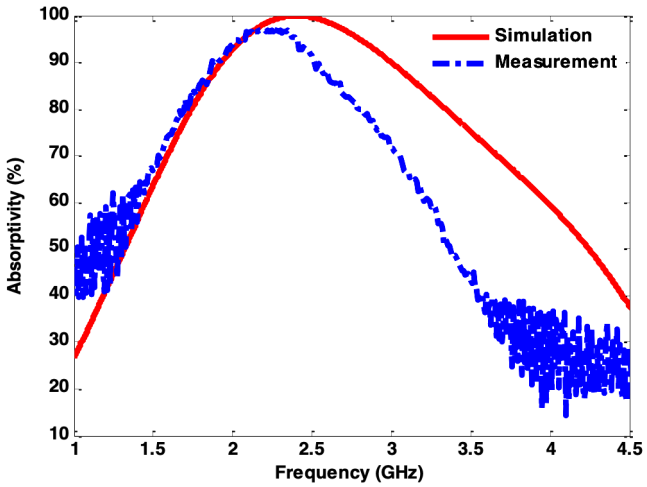

FIGURE 14. Simulated and measured Absorptivity response under normal incidence

The comparison between the proposed MM absorber and earlier wideband MM absorber structures is presented in Table II. The proposed MM absorber's unit cell achieves a significant 90% relative bandwidth. Furthermore, it performs well at various polarizations and incident angles.

TABLE II.
PROPOSED WORK COMPARED WITH PREVIOUS WIDEBAND MM ABSORBERS

Ref.	*Years*	*Relative Absorption bandwidth < 90% Frequency range*	*Dielectric material*	*Oblique angle stability*	*Polarization insensitive*
[38]	2017	16 % 840-990 MHz	FR4, air	30	NA
[49]	2015	Very narrow 2.4 GHz	FR4, air	NA	No
[50]	2022	44.5% (8.9 -14 GHz)	PVC+ OCA+PET+ ITO resistive film	60	yes
[51]	2015	11.3% (12.5 - 14 GHz)	FR4	60	Yes
[52]	2023	22% 24 – 26 GHz	FR4	30	Yes
[53]	2021	40% 20 – 30 GHz	FR4	40	No
[54]	2023	28% 21.2 – 28.2 GHz	FR4	60	Yes
This work	-	42.6% (1.94- 2.99 GHz)	FR4, air	75	Yes

IV. CONCLUSION

This paper describes and evaluates a wide-angle, polarization-insensitive MM absorber in the ISM band (2.4 GHz). The proposed MM absorber comprises four metallic sectors printed on a low-cost FR-4 substrate. The numerical results demonstrate that the proposed absorber exhibits a wideband absorption bandwidth exceeding 90% within the frequency band of 1.94 GHz to 2.99 GHz. The distributions of the E-field, H-field, and surface currents are discussed to understand the wide absorption mechanism better. The numerical analyses of the proposed absorber confirm its insensitivity to EM waves in both TE and TM polarizations. Furthermore, it maintains a strong absorption rate exceeding 90% even at TE polarization incidence angles of 60^{o}. The proposed absorber has been fabricated to validate the simulation results, and experimental measurements of the

reflection coefficient S11 confirm a correspondence between the simulated and actual absorption characteristics.
Based on the above outcomes, the proposed absorber is a promising choice for microwave applications, including EM protection and satellite stealth.

ACKNOWLEDGMENT

The authors would like to acknowledge the support provided by UniversitiTun Hussein Onn Malaysia (UTHM) and Universiti Teknikal Malaysia Melaka (UTeM) for their contribution to this research.

REFERENCES

[1] C. Caloz and T. Itoh, Electromagnetic metamaterials: transmission line theory and microwave applications. John Wiley & Sons, 2005.

[2] S. S. Islam, M. R. I. Faruque, and M. T. Islam, "A near zero refractive index metamaterial for electromagnetic invisibility cloaking operation," Materials (Basel)., vol. 8, no. 8, pp. 4790–4804, 2015, doi: 10.3390/ma8084790.

[3] Y. Roh et al., "Terahertz imaging with metamaterials for biological applications," Sensors Actuators B Chem., vol. 352, no. P1, p. 130993, Feb. 2022, doi: 10.1016/j.snb.2021.130993.

[4] K. Aydin, I. Bulu, and E. Ozbay, "Subwavelength resolution with a negative-index metamaterial superlens," Appl. Phys. Lett., vol. 90, no. 25, pp. 2005–2008, Jun. 2007, doi: 10.1063/1.2750393.

[5] Y. I. Abdulkarim et al., "Design and study of a metamaterial based sensor for the application of liquid chemicals detection," J. Mater. Res. Technol., vol. 9, no. 5, pp. 10291–10304, Sep. 2020, doi: 10.1016/j.jmrt.2020.07.034.

[6] Y. Liu, D. Zheng, Q. Feng, and Y.-S. Lin, "Electrothermally controllable terahertz metamaterial for sensing application," Sensors Actuators A Phys., vol. 344, no. May, p. 113667, Sep. 2022, doi: 10.1016/j.sna.2022.113667.

[7] M. Amiri, F. Tofigh, N. Shariati, J. Lipman, and M. Abolhasan, "Review on Metamaterial Perfect Absorbers and Their Applications to IoT," IEEE Internet Things J., vol. 4662, no. c, pp. 1–1, 2020, doi: 10.1109/jiot.2020.3025585.

[8] A. A. G. Amer, S. Z. Sapuan, N. Nasimuddin, and M. F. Hassan, "A Broadband Wide-Angle Metasurface Absorber for Energy Harvesting Applications," in 2021 International Conference of Technology, Science and Administration (ICTSA), Mar. 2021, no. April, pp. 1–4. doi: 10.1109/ICTSA52017.2021.9406540.

[9] A. A. G. Amer, S. Z. Sapuan, and Nasimuddin, "Multi-band Metasurface Microwave Absorber Based on Square Split-Ring Resonator Structure," in Lecture Notes in Electrical Engineering, vol. 770, Springer, Singapore, 2022, pp. 373–382. doi: 10.1007/978-981-16-2406-3_29.

[10] S. Liao, J. Sui, and H. Zhang, "Switchable ultra-broadband absorption and polarization conversion metastructure controlled by light," Opt. Express, vol. 30, no. 19, pp. 34172–34187, 2022, doi: 10.1364/oe.472336.

[11] Y. Li, L. Zeng, H. Zhang, D. Zhang, K. Xia, and L. Zhang, " Multifunctional and tunable metastructure based on VO 2 for polarization conversion and absorption ," Opt. Express, vol. 30, no. 19, p. 34586, 2022, doi: 10.1364/oe.470910.

[12] A. A. G. Amer, S. Z. Sapuan, and A. Y. I. Ashyap, "Efficient metasurface for electromagnetic energy harvesting with high capture efficiency and a wide range of incident angles," J. Electromagn. Waves Appl., pp. 1–12, Sep. 2022, doi: 10.1080/09205071.2022.2128898.

[13] A. A. G. Amer et al., "Dual-Band, Wide-Angle, and High-Capture Efficiency Metasurface for Electromagnetic Energy Harvesting," Nanomaterials, vol. 13, no. 13, p. 2015, Jul. 2023, doi: 10.3390/nano13132015.

[14] A. A. Ghaleb Amer, S. Z. Sapuan, and N. Nasimuddin, "Wide-Coverage Suspended Metasurface Energy Harvester for ISM Band Applications," in 2021 IEEE 19th Student Conference on Research and Development (SCOReD), Nov. 2021, pp. 87–90. doi: 10.1109/SCOReD53546.2021.9652779.

[15] T. M. Kollatou, A. I. Dimitriadis, S. D. Assimonis, N. V Kantartzis, and C. S. Antonopoulos, "A FAMILY OF ULTRA-THIN, POLARIZATION-INSENSITIVE, MULTI-BAND, HIGHLY ABSORBING METAMATERIAL STRUCTURES," Prog. Electromagn. Res., vol. 136, no. January, pp. 579–594, 2013, doi: 10.2528/PIER12123106.

[16] Y. Jang, M. Yoo, and S. Lim, "Conformal metamaterial absorber for curved surface," Opt. Express, vol. 21, no. 20, p. 24163, Oct. 2013, doi: 10.1364/OE.21.024163.

[17] Y. Naito and K. Suetake, "Application of ferrite to electromagnetic wave absorber and its characteristics," IEEE Transactions on Microwave Theory and Techniques, vol. 19, no. 1. pp. 65–72, Jan. 1971. doi: 10.1109/TMTT.1971.1127446.

[18] N. I. Landy, S. Sajuyigbe, J. J. Mock, D. R. Smith, and W. J. Padilla, "Perfect Metamaterial Absorber," Phys. Rev. Lett., vol. 100, no. 20, p. 207402, May 2008, doi: 10.1103/PhysRevLett.100.207402.

[19] F. Dincer, M. Karaaslan, E. Unal, O. Akgol, and C. Sabah, "Design of Polarization- and Incident Angle-Independent Perfect Metamaterial Absorber with Interference Theory," J. Electron. Mater., vol. 43, no. 11, pp. 3949–3953, Nov. 2014, doi: 10.1007/s11664-014-3316-x.

[20] M. R. Soheilifar, R. A. Sadeghzadeh, and H. Gobadi, "Design and fabrication of a metamaterial absorber in the microwave range," Microw. Opt. Technol. Lett., vol. 56, no. 8, pp. 1748–1752, Aug. 2014, doi: 10.1002/mop.28437.

[21] B. Ni, X. S. Chen, L. J. Huang, J. Y. Ding, G. H. Li, and W. Lu, "A dual-band polarization insensitive metamaterial absorber with split ring resonator," Opt. Quantum Electron., vol. 45, no. 7, pp. 747–753, Jul. 2013, doi: 10.1007/s11082-013-9676-2.

[22] S. Ramya and I. Srinivasa Rao, "DESIGN OF POLARIZATION-INSENSITIVE DUAL BAND METAMATERIAL ABSORBER," Prog. Electromagn. Res. M, vol. 50, no. July, pp. 23–31, 2016, doi: 10.2528/PIERM16070501.

[23] K. Majeed, S. A. Niazi, O. Altintas, M. A. Baqir, M. Karaslaan, and U. C. Hasar, "Multiband polarization-insensitive cartwheel metamaterial absorber," J. Mater. Sci., vol. 57, no. 46, pp. 21392–21401, 2022, doi: 10.1007/s10853-022-07975-2.

[24] E. Karakaya, F. Bagci, S. Can, A. E. Yilmaz, and B. Akaoglu, "Four-band electromagnetic energy harvesting with a dual-layer metamaterial structure," Int. J. RF Microw. Comput. Eng., vol. 29, no. 1, p. e21644, Jan. 2019, doi: 10.1002/mmce.21644.

[25] R. M. H. Bilal, M. A. Baqir, P. K. Choudhury, M. M. Ali, A. A. Rahim, and W. Kamal, "Polarization-insensitive multi-band metamaterial absorber operating in the 5G spectrum," Optik (Stuttg)., vol. 216, no. May, p. 164958, 2020, doi: 10.1016/j.ijleo.2020.164958.

[26] M. Huang, J. Yang, S. Jun, S. Mu, and Y. Lan, "Simulation and Analysis of a Metamaterial Sensor Based on a Microring Resonator," Sensors, vol. 11, no. 6, pp. 5886–5899, May 2011, doi: 10.3390/s110605886.

[27] H. Xiong, J. S. Hong, C. M. Luo, and L. L. Zhong, "An ultrathin and broadband metamaterial absorber using multi-layer structures," J. Appl. Phys., vol. 114, no. 6, 2013, doi: 10.1063/1.4818318.

[28] S. J. Li, X. Y. Cao, J. Gao, T. Liu, Y. J. Zheng, and Z. Zhang, "Analysis and Design of Three-Layer Perfect Metamaterial-Inspired Absorber Based on Double Split-Serration-Rings Structure," IEEE Trans. Antennas Propag., vol. 63, no. 11, pp. 5155–5160, 2015, doi: 10.1109/TAP.2015.2475634.

[29] S. J. Li et al., "Ultra-wideband and Polarization-Insensitive Perfect Absorber Using Multilayer Metamaterials, Lumped Resistors, and Strong Coupling Effects," Nanoscale Res. Lett., vol. 13, 2018, doi: 10.1186/s11671-018-2810-0.

[30] M. Yoo, H. K. Kim, and S. Lim, "Angular- and Polarization-Insensitive Metamaterial Absorber Using Subwavelength Unit Cell in Multilayer Technology," IEEE Antennas Wirel. Propag. Lett., vol. 15, pp. 414–417, 2016, doi: 10.1109/LAWP.2015.2448720.

[31] L. Li, J. Wang, H. Du, J. Wang, S. Qu, and Z. Xu, "A band enhanced metamaterial absorber based on E-shaped all-dielectric resonators," AIP Adv., vol. 5, no. 1, 2015, doi: 10.1063/1.4907050.

[32] D. Kundu, A. Mohan, and A. Chakraborty, "Ultrathin polarization independent absorber with enhanced bandwidth by incorporating giusepe peano fractal in square ring," Microw. Opt. Technol. Lett., vol. 57, no. 5, pp. 1072–1078, May 2015, doi: 10.1002/mop.29020.

[33] S. Guo, C. Hu, and H. Zhang, "Unidirectional ultrabroadband and wide-angle absorption in graphene-embedded photonic crystals with the cascading structure comprising the Octonacci sequence," J. Opt. Soc. Am. B, vol. 37, no. 9, p. 2678, 2020, doi: 10.1364/josab.399048.

[34] H. Pan and H. Zhang, "Broadband Polarization-Insensitive Coherent Rasorber in Terahertz Metamaterial with Enhanced Anapole Response and Coupled Toroidal Dipole Modes," Adv. Opt. Mater., vol. 10, no. 2, p. 2101688, 2022.

[35] W. Yuan and Y. Cheng, "Low-frequency and broadband metamaterial absorber based on lumped elements: design, characterization and experiment," Appl. Phys. A Mater. Sci. Process., vol. 117, no. 4, pp. 1915–1921, 2014, doi: 10.1007/s00339-014-8637-3.

[36] M. Bağmancı, M. Karaaslan, O. Altıntaş, F. Karadağ, E. Tetik, and M. Bakır, "Wideband metamaterial absorber based on CRRs with lumped elements for microwave energy harvesting," J. Microw. Power Electromagn. Energy, vol. 52, no. 1, pp. 45–59, Jan. 2018, doi: 10.1080/08327823.2017.1405471.

[37] K. Chen, X. Luo, G. Ding, J. Zhao, Y. Feng, and T. Jiang, "Broadband microwave metamaterial absorber with lumped resistor loading," EPJ Appl. Metamaterials, vol. 6, pp. 1–7, 2019, doi: 10.1051/epjam/2018011.

[38] W. Zuo, Y. Yang, X. He, D. Zhan, and Q. Zhang, "A miniaturized metamaterial absorber for ultrahigh-frequency RFID system," IEEE Antennas Wirel. Propag. Lett., vol. 16, pp. 329–332, 2017, doi: 10.1109/LAWP.2016.2574885.

[39] M. Yoo and S. Lim, "Polarization-independent and ultrawideband metamaterial absorber using a hexagonal artificial impedance surface and a resistor-capacitor layer," IEEE Trans. Antennas Propag., vol. 62, no. 5, pp. 2652–2658, 2014, doi: 10.1109/TAP.2014.2308511.

[40] M. Amiri, F. Tofigh, N. Shariati, J. Lipman, and M. Abolhasan, "Miniature tri-wideband Sierpinski-Minkowski fractals metamaterial perfect absorber," IET Microwaves, Antennas Propag., vol. 13, no. 7, pp. 991–996, 2019, doi: 10.1049/iet-map.2018.5837.

[41] S. Kalraiya, R. K. Chaudhary, and M. A. Abdalla, "Design and analysis of polarization independent conformal wideband metamaterial absorber using resistor loaded sector shaped resonators," J. Appl. Phys., vol. 125, no. 13, 2019, doi: 10.1063/1.5085253.

[42] Q. Wang and Y. Cheng, "Compact and low-frequency broadband microwave metamaterial absorber based on meander wire structure loaded resistors," AEU - Int. J. Electron. Commun., vol. 120, p. 153198, 2020, doi: 10.1016/j.aeue.2020.153198.

[43] S. Fan and Y. Song, "Ultra-wideband flexible absorber in microwave frequency band," Materials (Basel)., vol. 13, no. 21, pp. 1–11, 2020, doi: 10.3390/ma13214883.

[44] D. T. Phan et al., "Lightweight, Ultra-Wideband, and Polarization-Insensitive Metamaterial Absorber Using a Multilayer Dielectric Structure for C- and X-Band Applications," Phys. Status Solidi Basic Res., vol. 258, no. 10, pp. 1–8, 2021, doi: 10.1002/pssb.202100175.

[45] S. Kalraiya, R. K. Chaudhary, and M. A. Abdalla, "Resistor loaded wideband conformal metamaterial absorber for curved surfaces application," AEU - Int. J. Electron. Commun., vol. 143, no. November 2021, p. 154033, 2022, doi: 10.1016/j.aeue.2021.154033.

[46] H. Chen, Y. Huang, G. Li, Q. He, J. Xie, and L. Deng, "Design and experimental validation of a low-profile wideband metamaterial absorber by characteristic modes analysis," Results Phys., vol. 28, p. 104684, 2021, doi: 10.1016/j.rinp.2021.104684.

[47] Y. Zhang, W. Yang, X. Li, and G. Liu, "Design and Analysis of a Broadband Microwave Metamaterial Absorber," IEEE Photonics J., vol. 15, no. 3, pp. 1–10, 2023, doi: 10.1109/JPHOT.2023.3277449.

[48] B. Khan, B. Kamal, S. Ullah, I. Khan, and J. A. Shah, "Design and experimental analysis of dual - band polarization converting metasurface for microwave applications," Sci. Rep., no. 0123456789, pp. 1–13, 2020, doi: 10.1038/s41598-020-71959-y.

[49] M. Bakir, M. Karaaslan, F. Dincer, K. Delihacioglu, and C. Sabah, "Perfect metamaterial absorber-based energy harvesting and sensor applications in the industrial, scientific, and medical band," Opt. Eng., vol. 54, no. 9, p. 097102, 2015, doi: 10.1117/1.oe.54.9.097102.

[50] X. Lei et al., "Design and Analysis of a Novel Compact Metamaterial Absorber Based on Double-Layer ITO Resistive Film for Improving Signal Integrity," IEEE Access, vol. 10, pp. 24067–24079, 2022, doi: 10.1109/ACCESS.2022.3155234.

[51] H. Zhai, C. Zhan, L. Liu, and Y. Zang, "Reconfigurable wideband metamaterial absorber with wide angle and polarization stability," Electron. Lett., vol. 51, no. 21, pp. 1624–1626, 2015, doi: 10.1049/el.2015.1557.

[52] M. L. Hakim, T. Alam, M. T. Islam, H. Alsaif, and M. S. Soliman, "Polarization-independent fractal square splits ring resonator (FSSRR) multiband metamaterial absorber/artificial magnetic conductor/sensor for Ku/K/Ka/5G (mm-Wave) band applications," Meas. J. Int. Meas. Confed., vol. 210, no. January, p. 112545, 2023, doi: 10.1016/j.measurement.2023.112545.

[53] R. M. H. Bilal et al., "Wideband Microwave Absorber Comprising Metallic Split-Ring Resonators Surrounded With E-Shaped Fractal Metamaterial," IEEE Access, vol. 9, pp. 5670–5677, 2021, doi: 10.1109/ACCESS.2020.3048927.

[54] L. Dewangan, M. S. Patinavalasa, J. Acharjee, Y. Solunke, S. Ghosh, and N. K. Mishra, "Broadband metamaterial absorber for stealth applications at K-band," AEU - Int. J. Electron. Commun., vol. 170, no. May, p. 154828, 2023, doi: 10.1016/j.aeue.2023.154828.

ABDULRAHMAN AHMED GHALEB AMER received the B.Sc. degree from the Department of Electrical and Electronic Engineering at Aleppo University, Syria, in 2012, followed by an M.Sc. degree from University Tun Hussein Onn Malaysia (UTHM) in 2017. Furthermore, he obtained his Ph.D. from University Tun Hussein Onn Malaysia (UTHM) in 2022. Currently, he holds a postdoctoral fellowship at University Tun Hussein Onn Malaysia (UTHM). His research interests encompass Radio Frequency (RF) Energy Harvesting, Electromagnetic Compatibility (EMC), Electromagnetic Energy Absorber/Harvester, as well as the analysis of metamaterial and metasurface for energy harvesting antennas and sensing.

SYARFA ZAHIRAH SAPUAN (Member, IEEE) received a B.Eng. (Hons.) in electrical engineering from KUiTTHO, (2006), and was born in Kuala Lumpur, Malaysia. She received her M.Sc. degree in communication eng. from Nanyang Technological University (NTU), Singapore, in 2009, and her Ph.D. from UTHM in 2014. She is currently an Assoc. Prof. at UTHM. She is a Railway EMC Consultant for MRT2 communication systems and LRT3 power systems, (PS&DS). She is also an EMC engineer for the signaling system for Bombardier Malaysia. She teaches EMC courses, EM theory, Applied Electromagnetic, Signaling, and Communications, etc. She is an expert in EMC with 16 years of experience. Previously, she was the principal researcher of the EMC Cluster under EMCenter, UTHM. She is involved with several EMC projects and consultations with Petronas Global Technical Solution and Rapid Rail Sdn. Bhd. etc. Her research interests include EMC, EMI, EMF radiation to humans, antenna calibration and design, and RF.

NURMIZA BINTI OTHMAN. (or N.B. Othman, or Nurmiza B. Othman) received the BSc. and MSc. degrees in Electrical and Electronic Engineering from Utsunomiya University, Japan, in 2007 and 2009, respectively. Then, she obtained the Ph.D in Electrical and Electronic Engineering from Kyushu University, Japan in 2014. Currently, she is a senior lecturer at the Department of Electronic Engineering, Universiti Tun Hussein Onn Malaysia, Malaysia. Her research interests include development of new sensing system by using electromagnetic approach for medical and agricultural applications. She is also actively involved in Non-destructive Testing (NDT) related research using Eddy Current techniques.

ALI AHMED SALEM (Member, IEEE) received the M.Eng. degree in electrical power engineering from University Tun Hussein Onn Malaysia (UTHM), in 2016, and the Ph.D. degree in high-voltage from the Faculty of Electrical Engineering, UTHM, in 2021. He has been a Postdoctoral Fellow with Universiti Teknologi Malaysia (UTM) Grantee for 2 years. Currently, he is a Senior Lecturer with the School of Electrical Engineering, Universiti Teknologi MARA (UiTM) Shah Alam. His current research interests include the condition monitoring of high voltage insulators and transformers.

Ahmed Jamal Abdullah Al-Gburi (Member-IEEE) received his M.Eng and Ph.D. degrees in Electronics and Computer Engineering (Telecommunication systems) from Universiti Teknikal Malaysia Melaka (UTeM), Malaysia, in 2017 and 2021, respectively. He is currently a senior lecturer at the Faculty of Electronics and Computer Technology and Engineering (FTKEK).

From December 2021 to March 2023, he served as a Postdoctoral Fellow with the Microwave research group (MRG) at UTeM. He is a member of the Board of Engineers Malaysia (BEM) and the International Association of Engineers (IAENG). In 2023, he was recognized as one of the top 2% scientists worldwide by Stanford University and published by Elsevier. He has authored and co-authored numerous journal articles and conference proceedings. His research interests encompass Microwave sensors, Metasurfaces, UWB antennas, array antennas, and miniaturized antennas for UWB and 5G applications. Ahmed has been awarded the Best Paper Award from the IEEE Community and has earned several gold, silver, and bronze medals in international and local competitions.

ZAHRILADHA ZAKARIA received the B. Eng. and M. Eng. in Electrical and Electronic Engineering from the Universiti Teknologi Malaysia in 1998 and 2004 respectively, and the PhD degree in Electrical & Electronic Engineering from the Institute of Microwaves and Photonics (IMP), University of Leeds, United Kingdom in 2010. From 1998 to 2002, he was with STMicroelectronics, Malaysia where he worked as Product Engineer.

He is currently a Professor at University Teknikal Malaysia Melaka (UTeM). His research interests include variety of RF/ microwave devices and he has published more than 350 scientific manuscripts. He holds 8 intellectual property rights, and he has won several awards, including gold medal during several research and innovation exhibitions at the national and international levels. Dr. Zakaria is an active reviewer for prominent journals and also the recipient of Top Research Scientist Malaysia (TRSM) 2021.